Computers and Concrete, Vol. 3, No. 4 (2006) 197-212
DOI: http://dx.doi.org/10.12989/cac.2006.3.4.197

Material modeling of steel fiber reinforced concrete

B. Thomée†, K. Schikora‡ and K.-U. Bletzinger‡†

Lehrstuhl für Statik, Technische Universität München, Arcisstr. 21, D-80333 München, Germany

(Received December 1, 2005, Accepted May 3, 2006)

Abstract. Modeling of physically non-linear behavior becomes more and more important for the analysis of SFRC structures in practical applications. From this point of view we will present an effective, three-dimensional constitutive model for SFRC, that is also easy to implement in commercial finite element programs. Additionally, the finite element analysis should only require standard material parameters which can be gained easily from conventional experiments or which are specified in appropriate building codes. Another important point is attaining the material parameters from experimental data. The procedures to determine the material parameters proposed in appropriate codes seem to be only approximations and are unsuitable for precise structural analysis. Therefore a finite element analysis of the test itself is used to get the material parameters. This process is also denoted as inverse analysis. The efficiency of the proposed constitutive model is demonstrated on the basis of numerical examples and their comparison to experimental results. In the framework of material parameter identification the idea of a new, indirect tension testing procedure, the “Modified Tension Test”, is adopted and extended to an easy-to-carry-out tension test for steel fiber reinforced concrete specimens.

Keywords: steel fiber reinforced concrete; constitutive model; material law; flow theory of plasticity; multisurface plasticity; localization; fracture energy; FEM; modified tension test.

1. Introduction

Modeling of physically nonlinear material behavior becomes more and more important for the analysis of SFRC structures. According to the new German code “DBV-Merkblatt: Stahlfaserbeton” (DBV 2001) as well as the new German concrete code DIN 1045-1 it is possible to determine stress resultants using a nonlinear analysis. From this point of view we will present an effective, three-dimensional constitutive model for SFRC, that is also easy to implement in commercial finite element programs. Additionally, the finite element analysis should only require standard material parameters which can be gained easily from conventional experiments or which are specified in appropriate building codes.

2. What is steel fiber reinforced concrete?

Concrete is characterized by excellent load carrying behavior in compression but also by brittle failure in tension. Steel fibers are added to improve certain properties. The main properties to be

† Research Assoicate, Corresponding Author, E-mail: thomee@bv.tum.de
‡ Professor, E-mail: schikora@bv.tum.de
‡† Chair of Structural Analysis, E-mail: kub@bv.tum.de

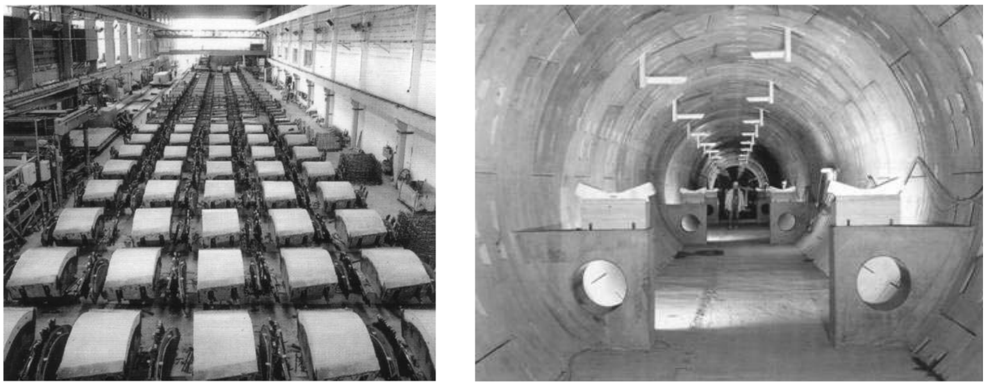

Fig. 1 Tunnel “Hofoldinger Stollen”- shield tunneling project with SFRC tunnel segments

mentioned are:

- Increasing ductility and blocking the crack growth.
  Due to the fibers, SFRC becomes a ductile material that has the ability to bear tensile stresses also in the presence of cracks.
- Increasing impact and explosion resistance.

Principal application areas of SFRC are:

- Tunneling: SFRC is applied both in terms of shotcrete linings and in terms of segmental tunnel linings. An example for the latter one, the tunnel “Hofoldinger Stollen” within the project of a new drinking water pipeline for Munich, is shown in Fig. 1. The tunnel is 17,5 km long and its diameter is 3,4 m. By using steel fibers (35-40 kg/m^3), conventional concrete reinforcement was not required.
- Industrial floors: Also in this case the steel fibers reduce or replace the conventional reinforcement.
- High performance concrete: The brittle failure of high performance concrete in compression can be improved by adding steel fibers. So called “fiber cocktails”, composed of e.g., steel- and polypropylen fibers, attain best effects.

In general it can be said that application of SFRC always makes sense when only small tensile stresses occur and cracking has to be reduced or avoided. Steel fibers are not able to replace conventional reinforcement in the case of large tensile or bending loading.

The fiber content of SFRC components usually varies between 20 kg/m^3 and 80 kg/m^3. The upper bound is about 120 kg/m^3 for reasons of workability and profitability.

3. Mechanical behavior of hardened steel fiber reinforced concrete

Mechanical behavior of hardened SFRC is strongly influenced by fiber content, type of fibers, fiber distribution and orientation (depending on the casting direction) and properties of the concrete matrix. Decreasing fiber content leads to a transition to the properties of plain concrete. Therefore, in the following we will deal with the properties of SFRC only in a qualitative way to explain the principle behavior.

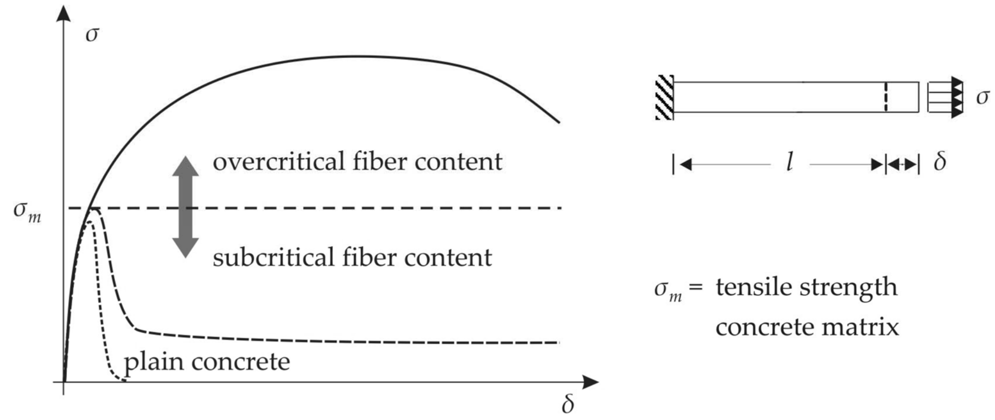

Fig. 2 Uniaxial tensile behavior of concrete and SFRC

3.1. Uniaxial tensile behavior

Fig. 2 shows the stress-elongation behavior of plain concrete and SFRC with subcritical and overcritical fiber content under uniaxial tension. The behavior of these three materials is almost identical before reaching the matrix strength. Up to about 60% of the matrix strength the stress-elongation relation is linear. Beyond this elastic limit micro-cracks are extending and the relationship becomes nonlinear.

As the matrix strength is reached, a completely different material behavior can be observed.

Plain concrete fails in a brittle manner and the tensile stresses are suddenly released. In the case of SFRC with overcritical fiber content the steel fibers are able to carry the whole tensile stress, even after the matrix has cracked. This is similar to the behavior of conventional minimal reinforced concrete. Consequently, the stress can be further increased. Critical fiber contents are about 100 kg/ m^3 to 200 kg/m^3 and they are, therefore, not of practical relevance. Most SFRC's in practical applications and which we consider here have subcritical fiber contents. In this case the available steel fibers are not able to carry the whole tensile stress, when the concrete matrix is cracking. This leads to a steep drop in the load bearing capacity in combination with a localized single crack after the tensile strength of the concrete matrix is reached. The sudden decrease is followed by a low level, post cracking plateau that results from continuous frictional pullout of the steel fibers. In this

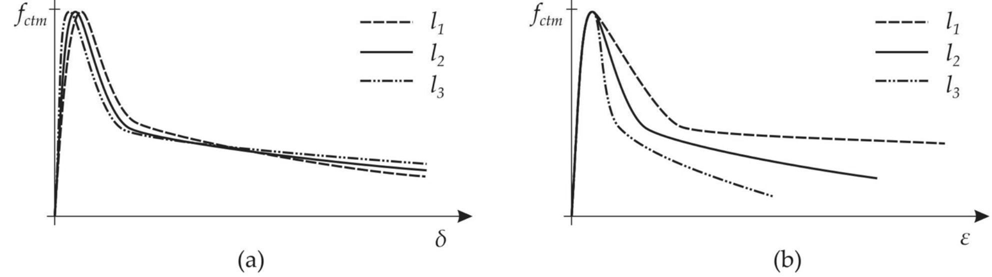

Fig. 3 The effect of the specimen length on the uniaxial stress-elongation (a) and stress-strain behavior (b)

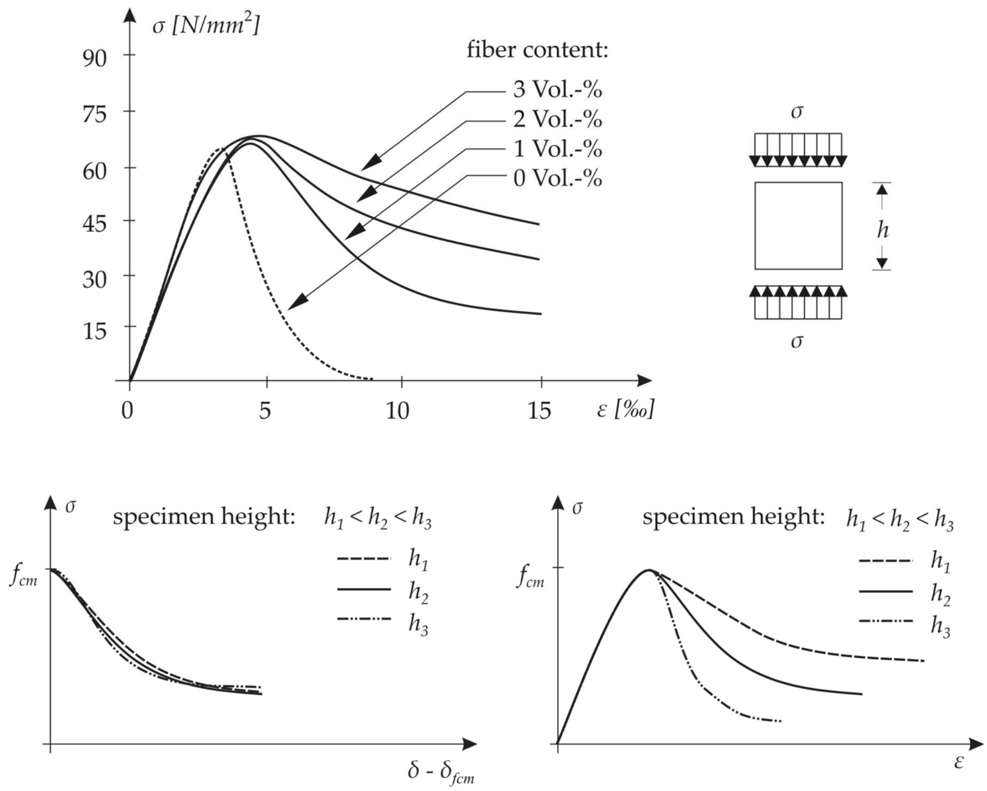

Fig. 4 Uniaxial compressive behavior of SFRC

case the typical behavior of localized cracking can be observed (Fig. 3). The stress strain relation depends on the length of the specimen whereas the stress-elongation relation is nearly independent. In order to obtain objective, mesh independent results in a finite element analysis this behavior has to be taken into account in the formulation of the material law.

3.2. Uniaxial compressive behavior

Fig. 4 shows that the addition of steel fibers will not strongly affect the compressive strength of the composite, but ductility increases significantly. The latter can be explained by the fact that the fibers prevent deformations in transverse direction. Also the phenomenon of strain localization can be observed (Tanigawa, *et al.* 1980).

4. Elasto-plastic constitutive model

4.1. Properties

The presented constitutive model is based on the flow theory of plasticity. Models based on this theory have already been used very successfully for plain concrete for example by Feenstra (1993) and Pravida (1999).

In order to model different material behavior of SFRC in compression and tension the yield surface is composed of two surfaces. The failure in tension is modeled by using a modified, smoothed Rankine criterion in combination with an isotropic softening law. To accomplish objective, mesh independent results the softening relation is based on the tensile fracture energy and an equivalent length which corresponds to a representative dimension of the finite element model. In compression a Drucker-Prager criterion with isotropic hardening and softening is used. The softening relation is also characterized by the compressive fracture energy. Thus a uniform treatment of the material behavior in tension and compression is guaranteed and numerical problems resulting from different constitutive models for cracking and crushing are avoided. By defining the yield surface in the three dimensional stress space the material model can be used for all kinds of stress states. Geometrically linear behavior is assumed. Time dependent phenomena like creep and shrinkage are not considered.

4.2. Algorithmic aspects

For integrating the incremental constitutive equations a fully implicit Euler backward scheme for multisurface plasticity is used. This algorithm was proposed by Simo & Hughes (1998).

To guarantee a quadratic rate of convergence in the global equilibrium iteration the consistent algorithmic tangent material stiffness matrix is used. It is derived from the linearized equations of the constitutive integration algorithm and is, therefore, consistent with the used integration scheme.

4.3. Mathematical model

A fundamental assumption within the framework of flow theory is the additive decomposition of the strain rate into a reversible elastic part and an irreversible plastic part:

$$\dot{\boldsymbol{\varepsilon}} = \dot{\boldsymbol{\varepsilon}}_{el} + \dot{\boldsymbol{\varepsilon}}_{pl} \tag{1}$$

The constitutive relation between the elastic strain rate and the stress rate is given by generalized Hooke's law:

$$\dot{\boldsymbol{\sigma}} = \mathbf{C}:\dot{\boldsymbol{\varepsilon}}_{el} = \mathbf{C}:(\dot{\boldsymbol{\varepsilon}} - \dot{\boldsymbol{\varepsilon}}_{pl}) \tag{2}$$

The yield function which governs the distinction between elastic and elastic-plastic load states is composed of m smooth yield surfaces and is expressed in the formulation for isotropic hardening:

$$f_i(\boldsymbol{\sigma}, \bar{\varepsilon}_{pi}) = F_i(\boldsymbol{\sigma}) - \bar{\sigma}_i(\bar{\varepsilon}_{pi}) = 0 \qquad i = 1, 2 \ldots m \tag{3}$$

The first part F_i transfers the general, 3d stress state into a so called effective stress which can be compared with yield stress $\bar{\sigma}_i$. The yield stress is a function depending on the internal variables. In this case the internal variable is the equivalent plastic strain $\bar{\varepsilon}_{pi}$ which controls the hardening and softening behavior.

Since the yield surface is composed of several surfaces bounded by edges, the direction of the plastic flow at these edges is not defined uniquely. The generalized flow rule, proposed by Koiter, serves as a remedy to treat the non-unique direction of the plastic strain rate:

$$\dot{\boldsymbol{\varepsilon}}_{pl} = \sum_{i=1}^{m} \dot{\lambda}_i \frac{\partial f_i(\boldsymbol{\sigma},\ \bar{\varepsilon}_{pi})}{\partial \boldsymbol{\sigma}} \quad \text{... associated case} \tag{4}$$

The isotropic hardening rule is based on a work hardening hypothesis. This implies that the rate of plastic work per unit volume of the general, multiaxial state is equal to that of the equivalent uniaxial state:

$$\dot{W}_{pi} = \bar{\sigma}_i\, \dot{\bar{\varepsilon}}_{pi} = \boldsymbol{\sigma} : \dot{\boldsymbol{\varepsilon}}_{pli} = \boldsymbol{\sigma} : \left(\dot{\lambda}_i \frac{\partial f_i(\boldsymbol{\sigma}, \bar{\varepsilon}_{pi})}{\partial \boldsymbol{\sigma}} \right) \tag{5}$$

If the function F_i is homogeneous of degree one in the stresses it follows, employing Euler's theorem, the equation for the evolution of the internal variables:

$$\dot{\bar{\varepsilon}}_{pi} = \dot{\lambda}_i \tag{6}$$

The consistency parameter $\dot{\lambda}_i$ and the rate of the yield function $\dot{f}_i$ have to fulfill the consistency condition:

$$\dot{f}_i \dot{\lambda}_i = 0 \tag{7}$$

For elastic-plastic loading, following from $\dot{\lambda}_i > 0$, the stress point has to be located on the yield surface and therefore:

$$\dot{f}_i(\boldsymbol{\sigma}, \bar{\varepsilon}_{pi}) = 0 \tag{8}$$

Assuming m active yield surfaces, the consistency parameters can be determined from the consistency condition:

$$\dot{\lambda}_i = \sum_{j=1}^{m} g^{ij} \left(\frac{\partial f_j(\boldsymbol{\sigma}, \bar{\varepsilon}_{pj})}{\partial \boldsymbol{\sigma}} : \mathbf{C} : \dot{\boldsymbol{\varepsilon}} \right) \quad \text{where} \quad g_{ij} = [g^{ij}]^{-1} = \frac{\partial f_i(\boldsymbol{\sigma}, \bar{\varepsilon}_{pi})}{\partial \boldsymbol{\sigma}} : \mathbf{C} : \frac{\partial f_j(\boldsymbol{\sigma}, \bar{\varepsilon}_{pj})}{\partial \boldsymbol{\sigma}} + \delta_{ij} \frac{\partial \bar{\sigma}_i}{\partial \bar{\varepsilon}_{pi}} \tag{9}$$

Introducing Eqs. (9) and (4) into Hooke's law (2) yields the elasto-plastic material tangent modulus which describes the relationship between total strain rate and stress rate:

$$\dot{\boldsymbol{\sigma}} = \frac{\left(\mathbf{C} - \sum_{i=1}^{m} \sum_{j=1}^{m} g^{ij} \left(\mathbf{C} : \frac{\partial f_i(\boldsymbol{\sigma}, \bar{\varepsilon}_{pi})}{\partial \boldsymbol{\sigma}} \right) \otimes \left(\mathbf{C} : \frac{\partial f_j(\boldsymbol{\sigma}, \bar{\varepsilon}_{pj})}{\partial \boldsymbol{\sigma}} \right) \right) : \dot{\boldsymbol{\varepsilon}}}{\mathbf{C}_{pl}} \tag{10}$$

4.4. Modified, smoothed, 3d Rankine criterion

According to the maximum-tensile-stress criterion of Rankine, also referred to as "tension cut off", failure respectively plastic flow takes place when the maximum principal stress reaches the tensile strength, respectively the yield stress. This criterion is generally accepted to model brittle failure such as cracking of concrete and SFRC (Hofstetter and Mang 1995).

In the principal stress space this criterion is composed of three planes perpendicular to the principal axes. At the corners of these planes the yield function is non-smooth and not differentiable. One

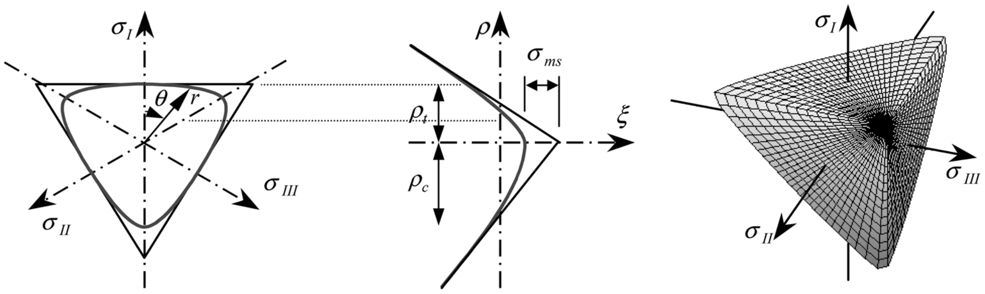

Fig. 5 Smoothed Rankine criterion - deviatoric section, meridian section and 3d principal stress space

way to handle non-smooth yield surfaces is using a multisurface plasticity, described above. An alternative way is smoothing the Rankine criterion and getting only one smooth surface for the tensile region. Furthermore the shape of the yield surface can thus be adapted to experimental results.

Smoothing is achieved by an elliptical fillet in the deviatoric plane and a hyperbolic fillet in the meridian plane (Fig. 5). The equation of this smooth criterion can be expressed as:

$$f_1(I_1, J_2, \theta, \bar{\varepsilon}_{p,1}) = \left(\left(\frac{2}{\sqrt{3}} \frac{\sqrt{J_2}}{r(\theta)} \right)^{2n} + \left(\frac{1}{\sqrt{3}} \sigma_{ms} \right)^{2n} \right)^{\frac{1}{2n}} + \alpha_R I_1 - \bar{\sigma}_1(\bar{\varepsilon}_{p,1}) \tag{11}$$

$r(\theta)$ describes the elliptical curve in the deviatoric section, depending on the lode angle θ. The apex angle in the meridian section can be controlled by means of the parameter α_R. Choosing α_R=1/3 leads to the angle of the Rankine criterion. The parameters σ_{ms} and n are used to smooth the meridian section. σ_{ms} reduces the tensile stress in the apex region and n governs the intensity of the smoothing. The greater n, the faster the curve approaches asymptotical to the non-smoothed curve.

4.5. Uniaxial hardening and softening relations

By means of the hardening and softening relations the constitutive model is adapted to uniaxial material behavior of SFRC.

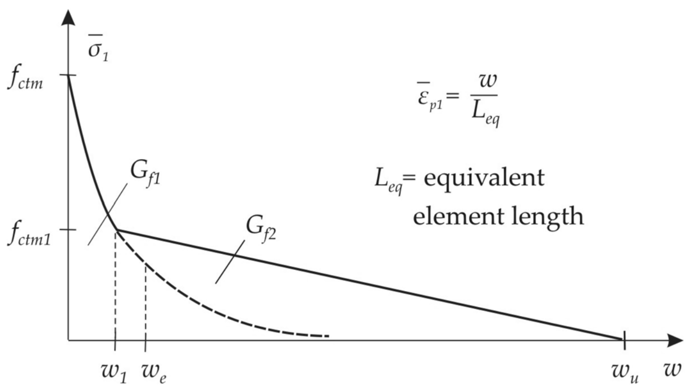

Fig. 6 Two-part stress-crack opening relation for SFRC

In tension linear-elastic material behavior is assumed before the tensile strength f_{ctm} is reached. After arriving at the peak stress, a sudden decrease in the stresses, followed by a low level, post cracking plateau that results from continuous pullout of the fibers, can be observed. To characterize this behavior a two-part stress-crack opening relation is used (Fig. 6). The first part is hardly affected by the fibers and therefore an exponential softening relation, proposed by Feenstra (1993), for plain concrete is assumed:

$$\bar{\varepsilon}_{p1} < \varepsilon_{R1}: \qquad \bar{\sigma}_1(\bar{\varepsilon}_{p1}) = f_{ctm} \cdot \exp\left(\frac{-\bar{\varepsilon}_{p1}}{\varepsilon_{Re}}\right) \tag{12}$$

where $\varepsilon_{Re} = \dfrac{G_{f1}}{f_{ctm}L_{eq}}$ and $\varepsilon_{R1} = -\ln\left(\dfrac{f_{ctm1}}{f_{ctm}}\right) \cdot \varepsilon_{Re}$

Material parameters for this purpose are the uniaxial tensile strength f_{ctm} and fracture energy G_{f1} for plain concrete. The second part of the relation is strongly influenced by the fibers. Here a linear softening relation is defined by the post-crack strength f_{ctm1} and the fracture energy of the steel fibers G_{f2}:

$$\varepsilon_{R1} < \bar{\varepsilon}_{p1} < \varepsilon_{Ru}: \qquad \bar{\sigma}_1(\bar{\varepsilon}_{p1}) = f_{ctm1} - \left(f_{ctm1} - \frac{(\bar{\varepsilon}_{p1} - \varepsilon_{R1})}{(\varepsilon_{Ru} - \varepsilon_{R1})}\right) \tag{13}$$

where $\varepsilon_{Ru} = \varepsilon_{R1} + \dfrac{2(G_{f2} + G'_{f1})}{f_{ctm1}L_{eq}}$

The crack opening is translated into an equivalent plastic strain by means of the equivalent element length L_{eq}.

The compressive strength of SFRC is more or less equal to the strength of plain concrete, but ductility increases significantly after cracking. This can be modeled by a quadratic hardening law

$$\bar{\varepsilon}_{p2} < \varepsilon_{DP,e}: \qquad \bar{\sigma}_2(\bar{\varepsilon}_{p2}) = \frac{f_{cm}}{3} \cdot \left(1 + 4\frac{\bar{\varepsilon}_{p2}}{\varepsilon_{DPe}} - 2\frac{\bar{\varepsilon}_{p2}^2}{\varepsilon_{DP,e}^2}\right) \tag{14}$$

and an exponential softening law (Fig. 7):

$$\bar{\varepsilon}_{p2} > \varepsilon_{DP,e}: \qquad \bar{\sigma}_2(\bar{\varepsilon}_{p2}) = f_{cm} \exp\left(\frac{(\bar{\varepsilon}_{p2} - \varepsilon_{DPe})^{\alpha}}{(\varepsilon_{DPu})^{\alpha}}\right) \tag{15}$$

$$\varepsilon_{DP,u} \text{ from } \frac{G_c}{L_{eq}} = \int_0^{\infty} \bar{\sigma}_2(\bar{\varepsilon}_{p2}) d\bar{\varepsilon}_{p2}$$

The ductile softening behavior in this model is controlled by the compressive fracture energy G_c. The parameter α can be used to adapt the shape of the softening branch.

In the diagram on the right hand side of Fig. 7 the provided fracture energy concept is compared with empirical stress-strain relations obtained from Tanigawa, *et al.* (1980) examining cylindrical and prismatic SFRC specimens with different slenderness ratios. It is obvious that the fracture energy concept is able to engage the influence of the specimen height on the stress-strain relation.

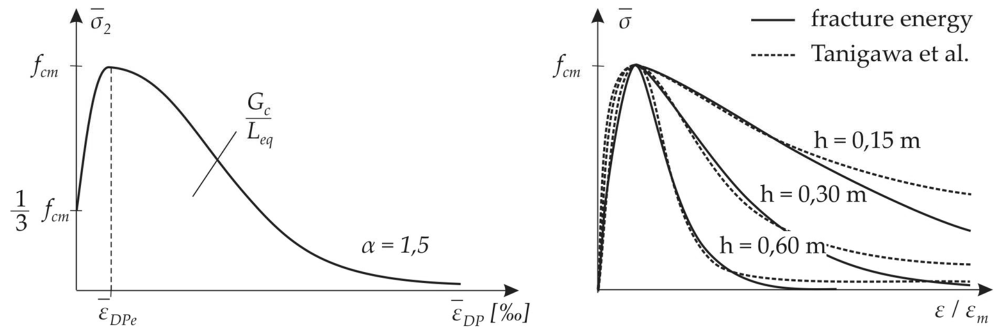

Fig. 7 Quadratic hardening and exponential softening relation and influence of the specimen height

5. Attaining the stress-crack opening relation

In theory, the uniaxial tensile test is the best testing method to determine the uniaxial post cracking behavior of SFRC, because the test results can be directly processed into a uniaxial stress-crack opening relation. On the other hand, there are some disadvantages like a complex test set-up and a high scatter in test results typical for this testing method. Hence the practical significance is limited and this type of experiment is not provided in appropriate codes or recommendation.

The standard testing procedure for SFRC prescribed for example in the German code DBV-Merkblatt “Stahlfaserbeton” (DBV 2001) is the four-point bending test. Therefore, the material parameters for the stress-crack opening relation are attained from these test results. The test, however, does not directly provide the stress-crack opening relation needed but a load-displacement relation. Codes propose to determine an elastic edge stress that is afterwards converted into an uniaxial stress by means of factors taking into account the non-linear stress distribution. Due to the highly nonlinear material behavior of SFRC this procedure is only an approximation. A more

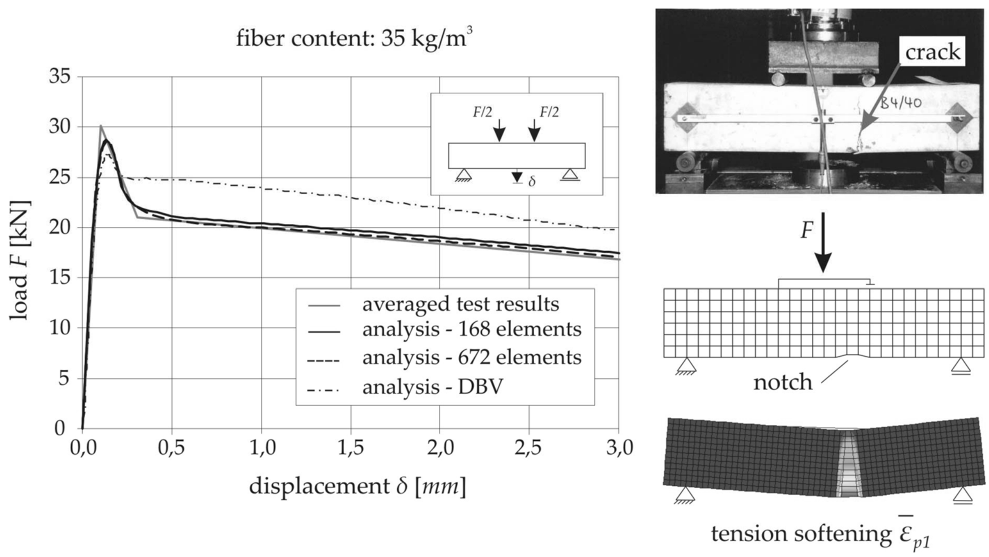

Fig. 8 FE-simulation of a four-point bending test

accurate way to determine the stress-crack opening relation is to perform a finite element analysis of the bending test. This process is also denoted as inverse analysis.

Fig. 8 shows a four-point bending test of a specimen with 35 kg/m^3 hooked-end steel wire fibers. The specimen fails along a single crack occurring at the weakest cross-section in the area with constant bending moment between the two upper point loads. In the finite element analysis the equivalent plastic strain $\bar{\varepsilon}_{p1}$ is a measure for the crack opening.

In the load-displacement diagram (Fig. 8) the gray line shows the averaged test results. The finite element analysis based on the approximate material parameters according to the DBV-Merkblatt "Stahlfaserbeton" (DBV 2001) is not able to describe the real structural behavior. Therefore the material parameters of the stress-crack opening relation must be determined via inverse analysis. The load-displacement curves calculated with these parameters are concordant to each other, despite of different meshes sizes. This indicates that the applied concept based on the fracture energy is able to cover the localization phenomenon of cracking in an objective way.

6. Numerical examples

6.1. Brazilian splitting tests

The finite element analysis of brazilian splitting tests on 15 cm large, SFRC cubes is based on the material parameters determined by the four-point bending test. The cube is modeled as a 2d plane stress problem with bilinear quadrilateral elements. The diagram in Fig. 9 shows the load plotted versus the strain measured by strain gages located at front and back of the cube. The computed load-strain curve shows good agreement with those measured in the experiments. The slightly stiffer behavior of the curve with the coarse mesh can be assigned to the discretization error. The kink at point A in the curves indicates exceeding the matrix tensile strength. The related load correlates to the maximum load carried by plain concrete specimens. Due to the ductile behavior of SFRC the load can be increased further.

6.2. Splitting tests on tunnel segments

In the range of the tunneling project "Hachinger Stollen" splitting tests on SFRC tunnel segments have been carried out to simulate the forces applied by the hydraulic jacks of the tunnel boring machine. For the finite element analysis one half of the segment is modeled with 2d plane stress bilinear quadrilateral elements as well as with 3d trilinear haxahedral solid elements.

The diagram in Fig. 10 shows the load-strain behavior from experiment as well as from simulation. The strain gages are located in middle and outside of the segment. Both simulation models are able to reproduce this behavior very well. Only the 3d model is able to show the differences between inside and outside of the segment. In addition the distribution of the equivalent plastic strain $\bar{\varepsilon}_{p1}$, a quantity for cracking and the equivalent plastic strain $\bar{\varepsilon}_{p2}$, a quantity for crushing reproduce the observed cracking and crushing pattern.

6.3. Nonlinear analysis of a tunnel lining

This example deals with the analysis of cross-sectional forces in the lining of a shield driven

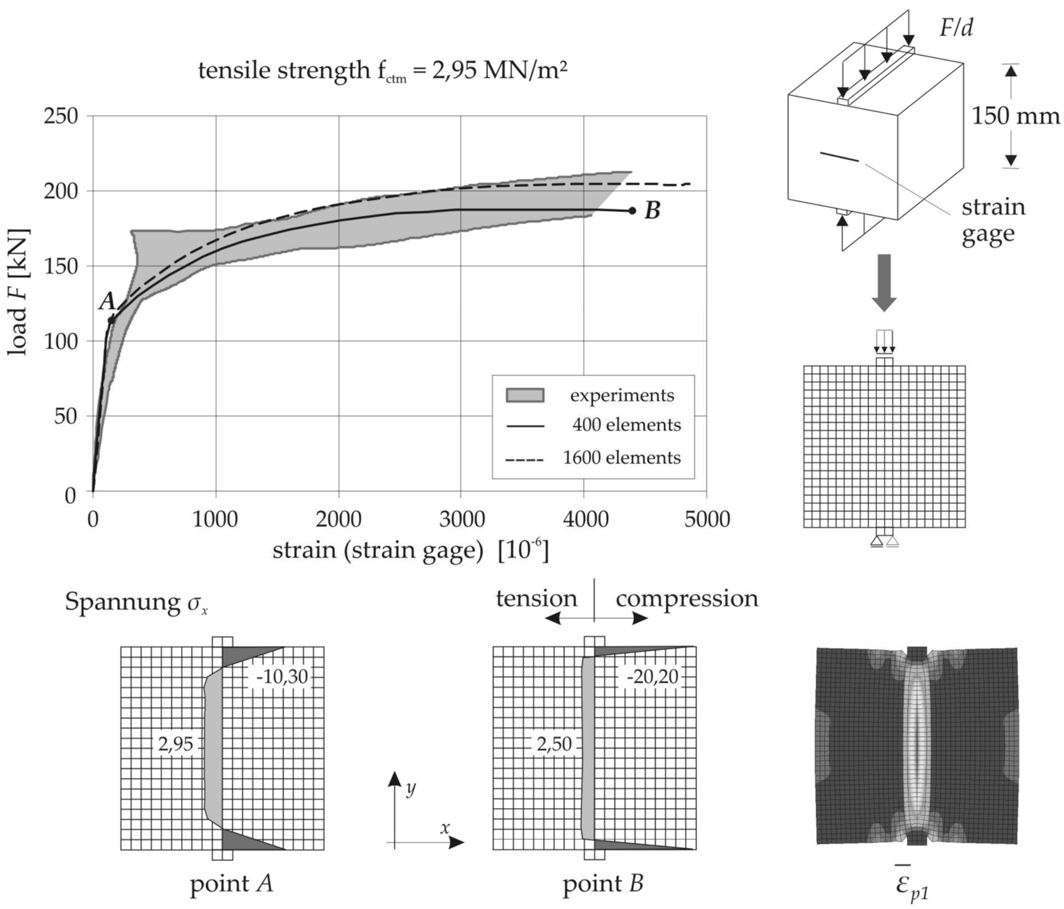

Fig. 9 Brazilian splitting tests on SFRC cubes

tunnel. One tunnel ring consists of four SFRC segments each. The special feature is a layer with rolling gravel in the crown area of the tunnel. The excavation process leads to a loss soil in the area. Consequently the loading in the roof segment increases due to missing bedding actions of the soil in this area. The stress resultants resulting from a linear analysis cannot be carried by the cross section.

For the analysis a 2d plane strain model is used. The soil is discretized with plane strain quadrilaterals in combination with a simple Drucker-Prager constitutive model. For the tunnel lining layered beam elements are used. The results of the nonlinear analysis compared with the linear analysis (Fig. 11) show that the normal forces, which are necessary for the load carrying behavior, remain roughly constant. On the contrary the bending moments are strongly reduced due to the nonlinear material behavior. Therefore only the physically nonlinear analysis with a proper constitutive model for SFRC enables the ultimate limit state.

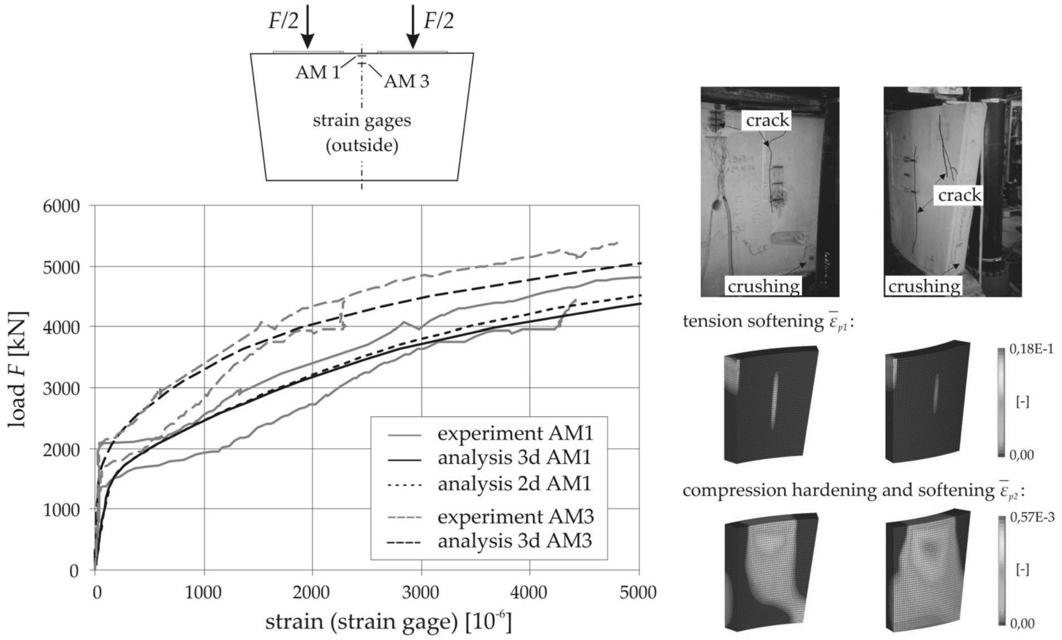

Fig. 10 Splitting test on SFRC tunnel segments

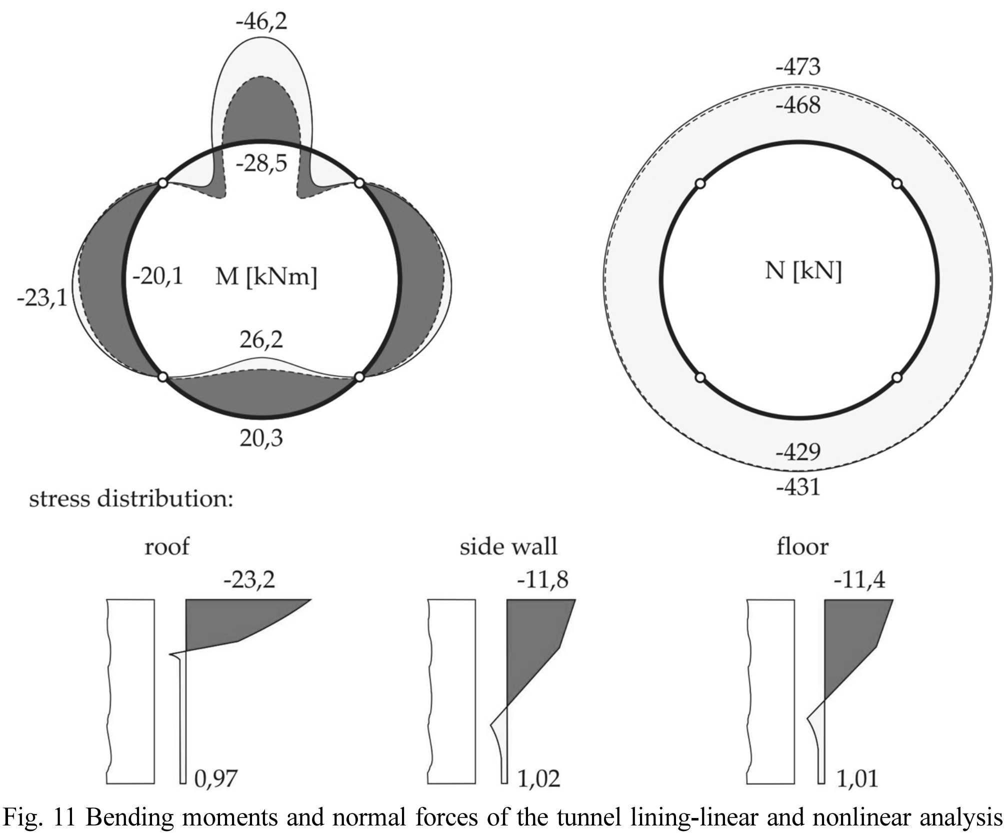

Fig. 11 Bending moments and normal forces of the tunnel lining-linear and nonlinear analysis

7. Modified tension test (MTT)

The “Modified Tension Test” represents a new, innovative and easy-to-carry out approach to the laboratory research of the uniaxial tensile strength. The MTT was developed at the institute for rock mechanics and tunneling at the TU Graz, Austria (Blümel 2000) for testing rock. The test uses a simple, cylindrical specimen that is over cored from the top and bottom by two axial core drill holes with different diameters (Fig. 12). After placing a load plate (top) and load ring (bottom), the sample is loaded in a standard testing device for compressive testing. Due to the axially symmetric

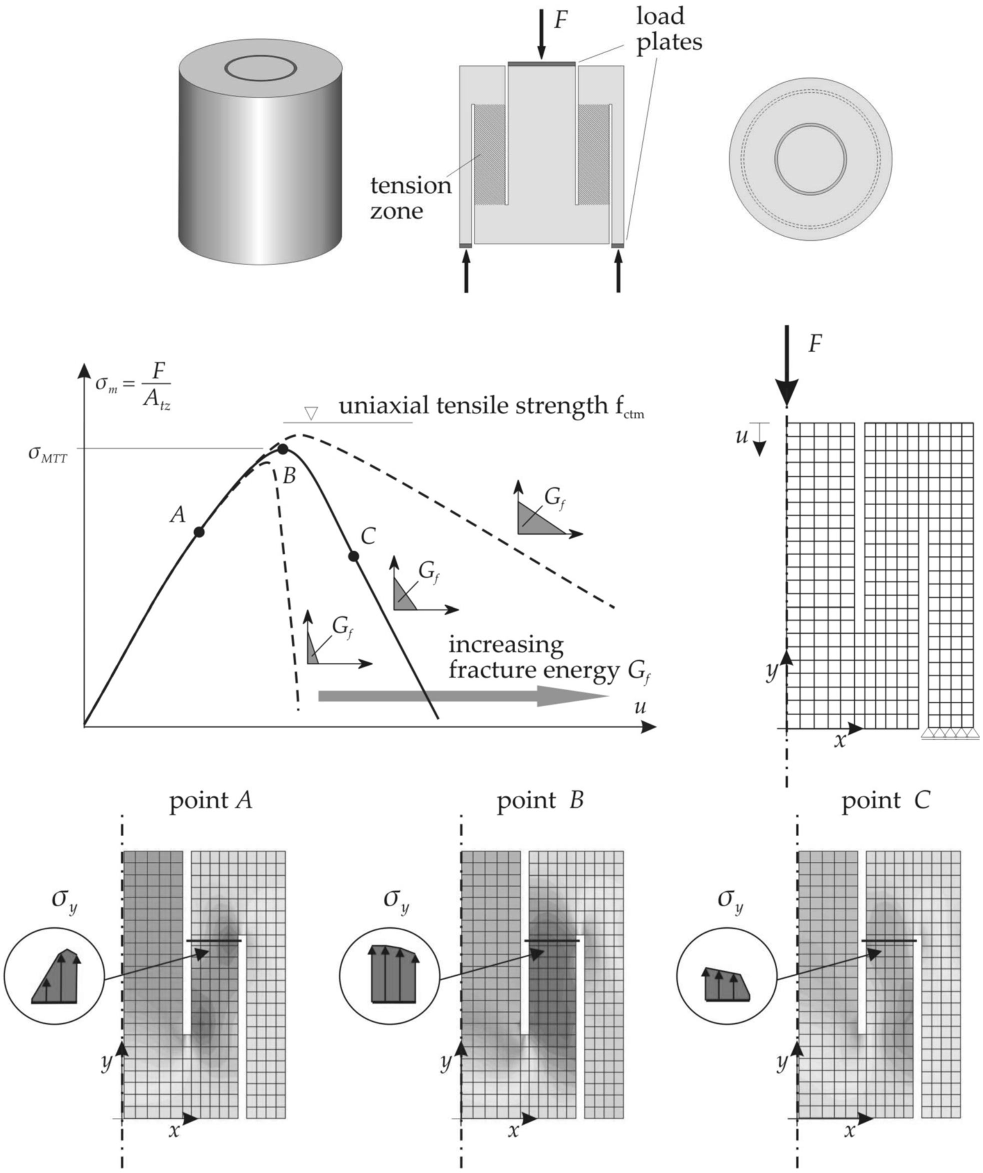

Fig. 12 MTT - Model for and results from the finite element analysis

geometry failure occurs by tension in the area in between the both overlapping core drill holes ("tension zone").

The averaged tensile strength σ_m is calculated from the compressive load F and the area of the tension zone A_{TZ} which depends on the radius r_1 and r_2 of the core holes:

$$\sigma_m = \frac{F}{A_{TZ}} = \frac{F}{r_1^2 \cdot \pi - r_2^2 \cdot \pi} \tag{16}$$

In order to further investigate stress distribution during testing, the MTT was simulated with a non-linear finite element calculation. The sample was modeled using four-node axisymmetric 2d solid elements (Fig. 12). Tensional softening is described by a simple linear branch. The qualitative results of the finite element calculation are illustrated in the upper left part of. The diagram shows the correlation between the mean tensional stress σ_m (Eq. (16)) and the axial deformation u.

In the lower part of Fig. 12, the distribution of stresses in y-direction is illustrated in cross sections through one half of the sample for 3 different stages of the test: (A) shows the stress distribution in the pre-failure area, (B) is at maximum load (failure point) and (C) shows the post-failure situation. The calculations give rise to the supposition, that the variable stress field in the pre-failure area (A) becomes more or less equally distributed in the tension zone when the failure point is reached (B). This effect shows to be largely influenced by the ductility of the material.

The maximum mean tensile strength MTT calculated from the finite element model is only a little lower than the implemented material tensile strength. The difference correlates to the ductility of the material which is described by the tensional fracture energy. With increasing ductility of the material, the calculated maximum mean tensile strength σ_{MTT} comes closer to the implemented material tensile strength due to a more equal stress distribution.

In particular for investigations on steel fiber reinforced concrete, constant stress distribution in the tension zone had to be assured for the whole pre and post-failure phase of the test. This was achieved using two additional core drill holes as shown in Fig. 13. Consequently, the central area of

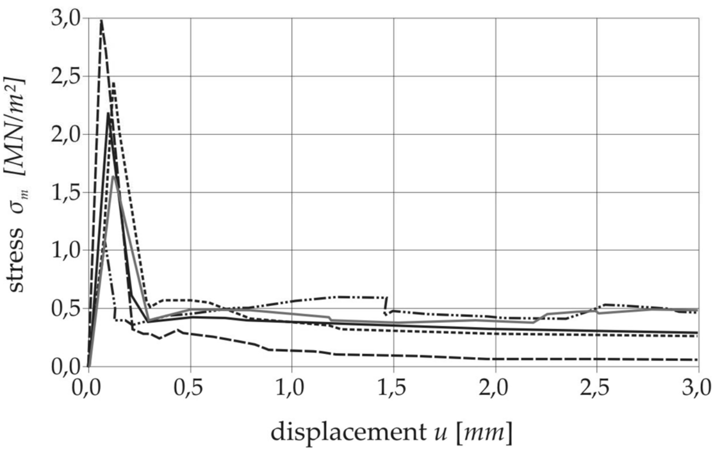

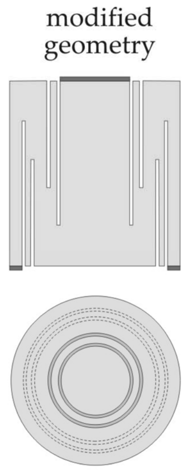

Fig. 13 MTT testing results for deformation-controlled tests on steel fiber reinforced concrete samples with modified geometry

the tension zone - with constant stress distribution - was further weakened and the initial crack was forced to propagate here. This testing setup has proved to deliver very good properties for steel fiber reinforced concrete. In combination with deformation-controlled testing and monitoring of the whole stress-strain path, it also allowed detailed and realistic investigation of the post-failure behavior, which for this type of concrete is defined by distinctive post-failure strength due to steel fibers being pulled out of the concrete matrix after failure (Fig. 13).

8. Conclusions

The constitutive model based on the flow theory of plasticity presented in this paper enables the physically nonlinear analysis of SFRC structures. It covers all important properties of hardened SFRC to describe material behavior in a phenomenological way on the macroscopic level. Additionally, the material law is easy to be implemented in commercial finite element programs and needs only material parameters that can be gained easily from conventional experiments or which are specified in appropriate building codes.

The presented constitutive model is based on the flow theory of plasticity. In order to model different material behavior of SFRC in compression and tension the yield surface is composed of two surfaces. The failure in tension is modeled by using a modified, smoothed Rankine criterion in combination with an isotropic softening law. In order to obtain objective, mesh independent results the softening relation is based on the tensile fracture energy and an equivalent length which corresponds to a representative dimension of the finite element model. For compression a Drucker-Prager criterion with isotropic hardening and softening is used. The softening relation is also characterized by the compressive fracture energy.

The material parameters for the stress-crack opening relation are attained from results of four point bending tests via inverse analysis. Based on these parameters actual SFRC structures are analyzed. The calculated load-strain curves of splitting tests on SFRC cubes and tunnel segments show good agreement to the ones measured in experiments. The nonlinear analysis of SFRC tunnel lining implies the possibility to reduce the bending moments and leads to more economical designs.

The Modified Tension Test is an innovative and easy-to-carry out testing procedure for determining the uniaxial tensile behavior of SFRC and shows a good ratio for required testing equipment and demands for the testing material. Therefore it is a good alternative to the direct tensile test, which is a rather difficult task.

References

Blümel, M. (2000), “Improved procedures for laboratory rock testing”, *Proceedings of the EUROCK 2000 Symposium*, Aachen, March, 573-578.

DBV Deutscher Beton- und Bautechnik-Verein e.V. (2001) “DBV-Merkblatt - Stahlfaserbeton”.

Feenstra, P.H. (1993), “Computational aspects of biaxial stress in plain and reinforced concrete”, Doctoral Dissertation, Technical University Delft.

Hofstetter, G. and Mang, H.A. (1995), *Computational Mechanics of Reinforced Concrete Structures,* Vieweg.

Plinninger, R.J., Wolski, K., Spaun, G., Thomée, B. and Schikora, K. (2003), “Experimental and model studies on the Modified Tension Test (MTT) - a new and simple testing method for direct tension tests”, *Proceedings of the Geotechnical Measurements and Modelling Congress*, Karlsruhe, September, 361-366.

Pravida, H. (1999), "Zur nichtlinearen adaptiven Finite-Element-Analyse von Stahlbetonscheiben", Doctoral Dissertation, Technical University Munich.
Simo, J.C. and Hughes, T.J.R. (1998), *Computational Inelasticity*; Springer.
Tanigawa, Y., Yamada, K. and Hatanaka, S. (1980), "Inelastic behavior of steel fiber reinforced concrete under compression", *Proceedings of the Int. Symp. Mat.Research Society: Advances in Cement-Matrix Composites*, Boston, 107-118.

NB